Solution of the two-center Dirac equation with 20-digit precision using the finite-element technique

O. Kullie [*]
Theoretical Physics, Institute for Physics, Department of Mathematics and Natural Science, Universität Kassel, 34132 Kassel, Germany

S. Schiller [†]
Institut für Experimentalphysik, Heinrich-Heine-Universität Düsseldorf, 40225 Düsseldorf, Germany

(Received 28 February 2022; accepted 20 April 2022; published 2 May 2022)

We present a precise fully relativistic numerical solution of the two-center Coulomb problem. The special case of unit nuclear charges is relevant for the accurate description of the H_2^+ molecular ion and its isotopologues, systems that are an active experimental topic. The computation utilizes the 2-spinor minmax approach and the finite-element method. The computed total energies have estimated fractional uncertainties of a few times 10^{-20} for unit charges and a bond length of 2 atomic units. The fractional uncertainty of the purely relativistic contribution is 1×10^{-17}. The result is relevant for future precision experiments, whereas at present the uncertainties arising from the quantum electrodynamic treatment of the rovibrational transition frequencies are dominant.

DOI: 10.1103/PhysRevA.105.052801

I. INTRODUCTION

There is currently considerable interest in precisely measuring the rotational and vibrational transitions in the molecular hydrogen ions and comparing the values with *ab initio* theory predictions [1]. Such comparisons allow a series of applications: determination of mass ratios, of nuclear charge radii, tests of wave mechanics, and search for fifth forces [2–4]. Disregarding hyperfine-structure contributions, the relativistic contributions are the largest ones beyond the Schrödinger energy. They make an important, easily measurable contribution to rotational and vibrational transition frequencies of the molecular hydrogen ions. For example, for the overtone vibrational transition $(v = 0, L = 0) \rightarrow (v' = 5, L' = 1)$ of HD^+, this contribution is $\simeq$4.0 GHz, or 1.5×10^{-5} relative to the transition frequency. Here v, L are the vibrational and rotational quantum numbers of the level. Today's experimental uncertainty of this transition frequency is of the order of 1 kHz, i.e., 2.5×10^{-7} of the relativistic contribution, and approximately 1×10^{-11} relative to the transition frequency itself [5]. There are excellent prospects for further reduction of the experimental uncertainty in the near future: this would be achieved using techniques already demonstrated for the precision spectroscopy of single atomic ions, that have reached uncertainties below the 1×10^{-17} level (see Ref. [6] for a review). Two aspects can be mentioned in this respect. First, the controlled trapping of single molecular hydrogen ions has recently been demonstrated [7] and, second, the systematic shifts of vibrational transitions have been analyzed theoretically and found to allow an uncertainty at the level below 1×10^{-16} [8]. Thus, it is clearly desirable to perform a highly precise theoretical evaluation of the relativistic contribution.

The currently employed approach to deal with the dominant relativistic effects is the perturbative evaluation of the Breit-Pauli Hamiltonian, with respect to the electronic wave function computed in the approximation of fixed nuclear charge centers [9]. This gives the relativistic shift of the order of α^2 compared to the nonrelativistic energy, the latter being close to -1 atomic unit (a.u.). Beyond this, the shift of relative order α^4 can also be computed perturbatively, with an appropriate formalism [10]. Finally, computations of the contribution of the order of α^6 have been available since the late 1980s.

In order to verify and extend the perturbation results, here we perform a high-precision numerical solution of the Dirac equation for the electron in the field of two static positive charges. We reduce the uncertainty of the relativistic shifts by a factor $>1 \times 10^7$ compared to the best previously published finite-element method (FEM) calculation, from 1×10^{-14} a.u. [11] to below 1×10^{-21} a.u.

The paper begins in Sec. II A with a brief introduction of the minmax approach for finding solutions of the Dirac equation, circumventing the issues found in other approaches. We also explain the iteration procedure and the nonrelativistic limit (Sec. II B). The implementation is discussed in Secs. II C and II D. Section III presents the computational aspects, including convergence of the FEM calculations and the treatment of the limiting cases of the hydrogen atom and of the nonrelativistic molecular hydrogen ion. The main results are contained in Sec. IV, viz., the relativistic shift as a function of the fine-structure constant and as a function of distance between the charge centers. Finally, Sec. V evaluates the consequences of the present treatment of the relativistic shifts on transition frequencies already measured for the molecular hydrogen ion.

[*]kullie@uni-kassel.de
[†]step.schiller@hhu.de

II. METHOD

We apply the method previously developed in the works of one of us (O.K.) [11–13]. A minmax principle is used that is based on the elimination of the small component from the Dirac equation, leading to a nonlinear eigenvalue problem that is solved iteratively. The main extension implemented is this work is the use of larger FEM order, larger number of grid points, and the use of quadruple precision (32 digits) in order to achieve a high numerical accuracy. Also, stringent tests are performed that allow one to determine the uncertainty of the energy values obtained in the numerical solution. Specifically, we obtain a highly accurate result for the $H_2{}^+$ system. We also show that the chosen relativistic treatment has an efficiency approaching that of the solution of the nonrelativistic Schrödinger equation.

A. Concept

A solution of the one-particle 4-spinor Dirac equation can be obtained from a stationarity principle for the functional $I = \langle\psi|\hat{H}|\psi\rangle - \varepsilon\langle\psi|\psi\rangle$, but one cannot apply a variational minimum principle as for the Schrödinger equation. However, there exists a minimum principle in the space of bound electronic states. The minmax principle (see [14] and references therein [15]) applies to the construction of the eigenvalues of an operator $\hat{H}$ that has a gap in its continuous spectrum (here from $-mc^2$ to mc^2) and that is unbounded from above and below. The principle considers the subspace of positronic states, F_-, and the subspace of electronic states, F_+, and requires a two-step search for extrema. The sequence of minmax level energies is given by

$$\lambda_k = \inf_{\substack{\dim G = k \\ G \text{ subspace of } F_+}} \sup_{\substack{\psi \neq |0\rangle \\ \psi \in (G \oplus F_-)}} \frac{\langle \psi \mid \hat{H} \mid \psi \rangle}{\langle \psi \mid \psi \rangle}, \tag{1}$$

where $F_+ \oplus F_-$ is an orthogonal decomposition of a well-chosen space of smooth square integrable functions and $\langle \psi \mid \hat{H} \mid \psi \rangle / \langle \psi \mid \psi \rangle$ is the Rayleigh quotient. It has been proven [14] that the sequence of the minmax energies λ_k equals the sequence of eigenvalues of $\hat{H}$ in the interval $(-mc^2, +mc^2)$. The minmax principle transforms the problem of finding a solution of the Dirac equation to a minimization (infimum) problem. It guarantees a solution of the Dirac equation in the space of the large component ϕ^+. The spectrum consists only of positive eigenvalues, i.e., the negative eigenvalues are eliminated and the spectrum is free from spurious states [14,15].

B. The minmax eigenvalue equation

The Dirac eigenvalue equation of the electron in a scalar potential V, $\hat{H}_D\,\psi = \varepsilon\psi$, with the 4-spinor ψ, can be written in the form

$$\begin{pmatrix} V & \hat{L}^\dagger \\ \hat{L} & V - 2mc^2 \end{pmatrix} \begin{pmatrix} \phi_+ \\ \phi_- \end{pmatrix} = \varepsilon \begin{pmatrix} \phi_+ \\ \phi_- \end{pmatrix}, \tag{2}$$

where we introduced the 2-spinors ϕ_+ and ϕ_- for the large and small component of ψ, respectively. $\hat{L} = -i\,c\,\hbar\,\sigma \cdot \nabla$, $\sigma = \sum_{k=1}^{3} \sigma_k\, e_k$, where σ_k are the Pauli matrices. ε is the eigenenergy that in the nonrelativistic limit corresponds to the eigenenergy of the Schrödinger equation. Rather than solving Eq. (2) directly, or operating with the functional I above, we proceed to reduce the 4-spinor treatment to a 2-spinor treatment. First, we eliminate the small component ϕ_- from Eq. (2), obtaining the differential ("strong") form

$$\hat{L}^\dagger \left(\frac{\hat{L}\,\phi_+}{\varepsilon + 2mc^2 - V} \right) = (\varepsilon - V)\,\phi_+. \tag{3}$$

In addition, we turn to a "weak" (integral) formulation that provides a good efficiency for FEM with large finite-element basis sets. It is obtained by multiplying both sides in Eq. (3) with $\phi_+^\dagger$ and integrating over the electron's coordinate space [14],

$$\int \frac{|\hat{L}\phi_+|^2}{\varepsilon + 2mc^2 - V} dr^3 = \int (\varepsilon - V)\,|\phi_+|^2 dr^3. \tag{4}$$

We now apply the minmax principle and seek the minimum value of ε. We expand the 2-spinor ϕ_+ over a set of basis functions with unknown coefficients. This set should be as large (complete) as possible. The vector of expansion coefficients will be denoted by $\overline{\phi}_+$. Variation of Eq. (4) with respect to the unknown coefficients in combination with the requirement that ε is stationary with respect to all coefficients leads to a matrix equation that determines the coefficients. It reads

$$\mathbf{M}(\varepsilon)\,\overline{\phi}_+ = \varepsilon\,\overline{\phi}_+. \tag{5}$$

Thus, the original 4-spinor Dirac equation has been transformed into a Schrödinger-like equation for the 2-spinor ϕ_+, but where the effective "Hamiltonian" $\mathbf{M}$ is eigenvalue dependent. The equation is nonlinear in the eigenvalue ε and therefore has to be solved by iteration. It can be shown that the solutions of this equation minimize the Rayleigh quotient over all electronic bound states of $\hat{H}_D$ [16].

It has been shown that an efficient approach consists of expanding the left-hand side of Eq. (4) in a series [14], as follows. We start with an approximate value ε^0 of an eigenvalue ε. For the iteration $j+1$ ($j = 0, \ldots, j_{\max}$), we expand the left-hand side as [17]

$$\begin{aligned} &\int \frac{|\hat{L}\phi_+|^2}{\varepsilon^j + 2mc^2 - V} dr^3 \\ &= \int \frac{|\hat{L}\phi+|^2}{\underbrace{(\varepsilon_0 + 2mc^2 - V)}_{g(\varepsilon_0)} + \Delta\varepsilon^j} dr^3 \\ &= \int \frac{|\hat{L}\phi_+|^2}{g(\varepsilon_0)} dr^3 + \sum_{k=1}^{k_{\max}} (-\Delta\varepsilon^j)^k \int \frac{|\hat{L}\phi_+|^2}{g(\varepsilon_0)^{k+1}} dr^3, \end{aligned} \tag{6}$$

with $\Delta\varepsilon^j = \varepsilon^j - \varepsilon_0$. The series expansion has the advantage that the iteration procedure reduces to solving successive eigenvalue problems. At iteration $j+1$, one computes the updated global matrix corresponding to the expression (6), $\mathbf{M}'(\varepsilon_0, \Delta\varepsilon^j)$. One then solves the conventional eigenvalue problem $\mathbf{M}'(\varepsilon_0, \Delta\varepsilon^j)\overline{\phi}_+ = \epsilon^{j+1}\overline{\phi}_+$. This is the computationally heaviest and therefore longest part of the numerical procedure. Another advantage of the series expansion is that the matrix elements for the individual terms in (6) need to be computed just once for a given grid, at the beginning of

the iteration. For explicit expressions of the elements of the matrix Hamiltonian $\mathbf{M}'$, we refer to Ref. [17].

The matrix equation is solved by an iterative method with a Cholesky decomposition [18]. In our method, only an open boundary condition is implemented so far, which has been found to work well.

The iteration process is stopped at $j = j_{\max}$ or when a required accuracy between successive iterations is reached. The series converges quickly and for atoms with small nuclear charge, only $k_{\max} = 3$ to 4 terms are needed. Typically, a small number of iterations is sufficient, $j_{\max} = 3$ for the $Z = 1$ case. For large-Z nuclei, usually $k_{\max} = 4$ to 9 terms are sufficient and $j_{\max} = 3$–7 remains small or moderate. For the nonrelativistic case $c \longrightarrow \infty$, the k expansion is unnecessary; see below.

In the FEM approach, one usually performs the computation for a series of grids with increasing number of elements and thus increasing number of basis functions. When one moves from one grid to the next finer grid, one uses as new start value ε^0 the solution $\varepsilon^{j_{\max}+1}$ found in the previous grid.

The 2-spinor formulation exhibits major advantages compared to the 4-spinor formulation: the number of matrix elements to be computed is a factor of 3 smaller and the solution of the matrix (by inverse vector iteration) requires a factor of 4 fewer operations. The reduced size of the problem enhances the computational performance and allows one to tackle larger problems [13,17].

Note that Eq. (4) can be written in the form

$$\int \frac{c^{-2}|\hat{L}\phi^+|^2}{[2m + (\varepsilon - V)/c^2]} = \int (\varepsilon - V)\,|\phi_+|^2 dr^3. \tag{7}$$

Therefore, in the nonrelativistic limit ($c \to \infty$), Eq. (4) turns into the Schrödinger equation, considering that $\hat{L}$ is proportional to c. Thus, we recognize that Eq. (4) exhibits similar properties to the Schrödinger equation. In practice, we calculate the nonrelativistic values by setting c to a large number, $c \geqslant 10^{15} (\alpha^2 \leqslant 10^{-30})$. In this limit, the small component ϕ_- becomes zero and the two components of ϕ_+ are then identical. The possibility of computing the nonrelativistic energy value in this way (i.e., using the same numerical procedures) leads to an important advantage: by subtracting it from the value for finite c, we can extract the relativistic *shift* with a better accuracy than the accuracy of the total (nonrelativistic plus relativistic shift) energy (see Sec. III).

We showed in previous work [13,19] that in the weak formulation, the 2-spinor fully relativistic FEM approach to the two-center Coulomb problem is numerically better behaved than the numerical solution of the 4-spinor Dirac equation. One finds some very desirable behaviors: the energy values converge from above with increasing grid size (finer subdivisions) and do not show the typical convergence from below or oscillatory convergence of the 4-spinor Dirac equation. This is a consequence of the elimination of the small component ϕ_-, which effectively projects the problem onto electronic states and leads to a second-order differential operator bounded from below.

C. Implementation

The Dirac Hamiltonian for a single particle of mass m in a two-center potential V is

$$\widehat{H}_D = c\,\widehat{\alpha}\cdot\widehat{\mathbf{p}} + mc^2\widehat{\beta} + V, \tag{8}$$
$$V = -\sum_{l=1}^{2} \frac{\hbar\, c\,\alpha\, Z_l}{|\mathbf{r} - \mathbf{R}_l|}.$$

Z_1, Z_2 are the charges of the two nuclei in units of the elementary charge, $\widehat{\alpha}$ and $\widehat{\beta}$ are the usual Dirac matrices, $\mathbf{r}$ is the position of the electron, $\widehat{\mathbf{p}}$ is the momentum operator, and $\mathbf{R}_l$ are the positions of the nuclei. α is the fine-structure constant. Alternatively, if atomic units are employed,

$$\widehat{H}_D = mc^2\alpha^2(\alpha^{-1}\widehat{\alpha}\cdot\widehat{\mathbf{p}}' + \alpha^{-2}\widehat{\beta} + V'), \tag{9}$$
$$V' = -\sum_{l=1}^{2} \frac{Z_l}{|\mathbf{r}' - \mathbf{R}'_l|}.$$

The primed quantities correspond to the case when coordinates and momenta are in atomic units. $m\alpha^2c^2$ is the atomic unit of energy.

The nonrelativistic energy is found from the difference between the total energy and the rest-mass energy $m\,c^2$, in the limit $c \to \infty$ of Eq. (8), or, equivalently, in the limit $\alpha = e^2/(4\pi\epsilon_0\hbar\,c) \to 0$ of Eq. (9). In both cases, the product $c\,\alpha$, i.e., the potential energy V, V' and the atomic energy unit, are to be kept constant. In the following, often c and α^{-1} are used synonymously; they are equal in an appropriate system of units. For the atomic case ($Z_2 = 0$), we consider different values of Z_1, in particular $Z_1 \gg 1$; see below.

For the two-center case, one has axial symmetry around the internuclear axis (the z axis) and favorably uses prolate spheroidal (elliptic spheroidal) coordinates ξ and η,

$$x = \frac{R}{2}u(\xi,\eta)\,\cos\varphi, \quad y = \frac{R}{2}u(\xi,\eta)\,\sin\varphi,$$
$$z = \frac{R}{2}\xi\cdot\eta, \text{ where } u(\xi,\eta) = \sqrt{(\xi^2-1)(1-\eta^2)}, \tag{10}$$

and R is the internuclear distance in atomic units. The electron's angular coordinate is φ. The distances between the electron and the nuclei are

$$r_1 = (\xi+\eta)\frac{R}{2}, \quad r_2 = (\xi-\eta)\frac{R}{2}. \tag{11}$$

The Coulomb singularity of point nuclei causes a singular behavior of the relativistic solutions at the position of the nuclei of the form $r_l^{-1+\gamma_{l,\kappa}}$, with $\gamma_{l,\kappa} = \sqrt{\kappa^2 - (\alpha Z_l)^2}$ and $\kappa = |j_z| + \frac{1}{2}$, $l = 1, 2$. This is well known from atomic calculations [20,21]. Thus, further singular coordinate transformations (whose back transform is nonanalytic) are needed to take care of this issue [11,12,17]. The transformation from ξ, η to s, t reads

$$\xi = 1 + c_1\sinh^{\nu}(s/2) + c_2\sinh^{(\nu+2)}(s/2)\cdots, \tag{12}$$
$$\eta = 1 - c_1\sin^{\nu}(t/2) + c_2\sin^{(\nu+2)}(t/2) - \cdots;$$
$$0 \leqslant s < \infty, \quad 0 \leqslant t \leqslant \pi,$$
$$\text{for } \nu = 2, 4, 6, 8, 10, \text{ with } c_i = 0 \quad \text{for } i > \frac{\nu}{2}.$$

The transformation regularizes the singularities at the nuclei by increasing the point density in the inner region. The higher ν, the denser the points near the nuclei to ensure a better approximation of the wave function. The coefficients and the details are given in Refs. [11,12]. As a result of this transformation, one can use a square grid over s and t.

A high value of ν (e.g., 6, 8) is needed for grids with a large number of points, which in turn enable a higher convergence order q for the energy and the full utilization of a FEM approximation of the order p. See below and Refs. [12,13,17].

Because of axial symmetry, the angular dependence is treated analytically by the ansatz,

$$\psi = \begin{pmatrix} \phi_+(s,t,\varphi) \\ \phi_-(s,t,\varphi) \end{pmatrix} = \begin{pmatrix} \phi^1(s,t)\cdot e^{i(j_z-1/2)\cdot\varphi} \\ \phi^2(s,t)\cdot e^{i(j_z+1/2)\cdot\varphi} \\ i\phi^3(s,t)\cdot e^{i(j_z-1/2)\cdot\varphi} \\ i\phi^4(s,t)\cdot e^{i(j_z+1/2)\cdot\varphi} \end{pmatrix}. \quad (13)$$

The wave function ψ is an eigenstate of the total angular momentum, and the good quantum number j_z is the z component of the total angular momentum.

In the present FEM treatment, the definition domain of s,t is subdivided into triangular elements e. Each component k of the relativistic wave function is approximated as

$$\phi^k(s,t) = G^k(s,t)\sum_e \sum_i^n d_i^{k,e} N_i^{k,e}(s,t), \quad (14)$$

where $G^k(s,t)$ are global functions, and the sums run over all elements e of the grid and over all n nodal points (s_i,t_i) of each element. $G^k(s_i,t_i)\,d_i^{k,e}$ is the value of the wave function at nodal point i. The shape functions $N_i^e(s,t)$ are zero outside the element e. Inside they are complete polynomials of the order of p in s,t [22], implementing a Lagrange-form interpolation. The values of the coefficients of the polynomials are determined by the conditions that $N_i^{k,e}(s_j,t_j)=\delta_{ij}$ for all nodal points i,j inside the element. In our FEM implementation, we use triangular Lagrangian-type elements with equidistant point distribution. The functions $G^k(s,t)$ account for the global behavior of the wave function, where $G_1^k(s,t)$ represents the angular momentum dependence and $G_2^k(s,t)$ expresses the singular behavior at the two nuclei. They are given by

$$\begin{aligned} G^k(s,t) &= G_1^k(s,t)\cdot G_2(s,t), \\ G_1^k(s,t) &= [(\xi^2-1)(1-\eta^2)]^{\frac{m_k}{2}} = R_\perp^{\frac{m_k}{2}}, \end{aligned} \quad (15)$$

$$\begin{aligned} m_{1,3} &= j_z - 1/2, \quad m_{2,4} = j_z + 1/2, \\ G_2(s,t) &= r_1^{-1+\gamma_{1,\kappa}}\cdot r_2^{-1+\gamma_{2,\kappa}}. \end{aligned} \quad (16)$$

Here, $R_\perp$ is the (perpendicular) distance to the internuclear axis. For larger Z, $\gamma_{l,k}$ becomes smaller and the singular behavior of the wave function is stronger, hence the convergence is less efficient. Indeed, as can be seen for the example hydrogenic atoms (Table III), the numerical precision decreases for higher atomic numbers. Still, introducing the singular coordinate transformation given by Eq. (12) guarantees a high convergence order because it allows one to describe the singularity of the wave function near the nuclei more accurately [20,23].

III. COMPUTATIONAL ASPECTS

A. Generalities

We compute the lowest-energy state of energy $\varepsilon_{1(1/2)g}$, i.e., with $j_z = 1/2$, and gerade symmetry g. The notation of the corresponding nonrelativistic state is $1\sigma_g$. We abbreviate the notation of the (exact) energy in atomic units by the shorthand $E_{\rm rel}$.

In all calculations, we use the FEM polynomial order $p = 10$. We run the calculation for different values of ν and size of the grid in order to achieve the best convergence. The size is defined by the size of the largest ellipse, $\xi = \xi_{\max} = \text{const}$, containing the grid elements. The size of the grid can alternatively be defined by $D_{\max}(\xi_{\max})$, defined as the distance between one of the centers to a point on the outermost ellipse $\xi_{\max}$, where this distance is perpendicular to the line between the two centers [19]. $D_{\max}$ values (given in atomic units) of approximately 30–50 are used. This should be compared to the most relevant value of the internuclear distance, $R = 2$, the approximate equilibrium bond length of the $H_2{}^+$ molecule. From this comparison, we see that the space around the nuclei considered in the calculation is large compared to the internuclear distance.

The largest number of grid points we were able to reasonably work with was $N = 32\,761$. As we show below, for the system $H_2{}^+$, a fractional uncertainty of the energy of the order of 10^{-20} is thereby achieved. For the relativistic shift, the absolute uncertainty is of the order of 10^{-22} atomic units, where we profit from an error cancellation concerning the nonrelativistic energy $E_{\rm nrel}$. Thus, this is a high-performance calculation. The computing time for the grid sequence up to 648/32 761 (see Table I) was 15–20 core-hours on a supercomputer. The code is not parallelized and runs on one core.

B. Convergence for the fully relativistic and the nonrelativistic case

We present in Table I the relativistic and nonrelativistic energy values $E_{\rm rel}(N)$, $E_{\rm nrel}(N)$ of $H_2{}^+$ in grids of different point number N, including their extrapolations to an infinite grid [19]. The relativistic shift $\Delta E_{\rm rel}$ (fourth column) is the difference, $E_{\rm rel} - E_{\rm nrel}$.

Performing an extrapolation is legitimate if the energy values exhibit a regular dependence on the grid size. This is the case for this problem if relevant parameters are chosen judiciously. For the computation reported in Table I, indeed, one notices that with increasing number of grid points (finer subdivision), the accuracy increases and convergence to the true value is from above, not only for the nonrelativistic case but also for the relativistic case. This behavior is known from previous treatments of the 2-spinor approach and is a major advantage of this method. As a guide to the eye, bold digits show the significant digits, but the actual uncertainty may be smaller than one unit of the last bold digit.

To test the convergence and confirm the accuracy of the result, we present in Fig. 1 a log-log plot of the errors $\delta E(N)$ of the energies and of the relativistic shift computed for a particular grid N, with respect to the extrapolated value. As can be seen in the red and blue line of the left panel, the convergence rate in the 2-spinor formulation is close to that

TABLE I. Energies of H_2^+ at $R = 2$ and for $\alpha^{-1} = 137.035999084$. All values in atomic units. The calculations utilize $\nu = 6$ and $D_{\max} = 50$. N_e, N are the numbers of the elements and grid points, respectively. Superscript [1] indicates values extrapolated over the sequence N_e. Bold digits are significant. Superscript [2] is with $\nu = 2$, and $D_{\max} = 50$; the relativistic shift is computed using the last relativistic energy value of column 2.

N_e/N	Relativistic, $E_{\rm rel}$	Nonrelativistic, $E_{\rm nrel}$	Rel. shift, $\Delta E_{\rm rel}$ (10^{-6})
8/441	**−1.102**2810444704063122 09	**−1.102**27360061312893971 01	**−7.**4438572773737249928
32/1681	**−1.10264157**5567778026666	**−1.10263420**902927647740 58	**−7.36653**850154926045
72/3721	**−1.1026415810**12739732920	**−1.1026342144**751026384076	**−7.3665376**3709451296
128/6561	**−1.1026415810324**0750588	**−1.1026342144947**767797576	**−7.3665376307**2611806
200/10201	**−1.1026415810325**76082616	**−1.1026342144949453**798398	**−7.3665376307027**7600
288/14641	**−1.1026415810325771**38209	**−1.1026342144949464**356152	**−7.3665376307025**9364
392/19881	**−1.1026415810325771**62741	**−1.1026342144949464**601360	**−7.3665376307026**0506
512/25921	**−1.1026415810325771**63917	**−1.1026342144949464**613087	**−7.3665376307026**0827
648/32761	**−1.1026415810325771640**97	**−1.1026342144949464**614889	**−7.3665376307026**0893
extrpl[1]	**−1.1026415810325771641**18	**−1.1026342144949464615**095	**−7.3665376307026090**1
extrpl[2]		**−1.1026342144949464615089689454**	**−7.3665376307026090**3

of the nonrelativistic Schrödinger equation [19]. This is the main result of the minmax concept.

When we choose a suitably large value of ν, the values converge extremely rapidly. The mean convergence is approximately $\sim N^{-8}$ considering all results from Table I. The convergence rate even appears to increase for the largest values of N used.

The accuracy in the FEM using polynomials of the order of p typically scales as $\sim N^{-p}$ with grid size. In our case, N can be made sufficiently large, but the singular behavior near the centers significantly reduces the efficiency of the FEM approximation. This can be controlled by the singular coordinates transformation given by Eq. (12), as already mentioned, but it is necessary to adapt the value of ν to the grid size. This issue is not so important in the nonrelativistic case because the wave function is finite at the nuclei. To illustrate this, we performed calculations for the same grids given in Table I, but with a lower value $\nu = 4$, and present the corresponding log-log plot in Fig. 1 (right).

For small grids, the error evolution is similar for both the relativistic and nonrelativistic values; here the distribution of the grid points is balanced between inner and outer regions. Then, for a larger number of grid points, the error caused by the relativistic singularity [Eq. (16)] becomes larger. This is because, for small ν, the points' density in the inner region is not sufficient to reproduce the singular behavior at the nuclei. The error of the FEM solution then does not decrease any more strongly with increasing grid size. In contrast, in the nonrelativistic case, the error continues to decrease strongly with increasing N.

Returning to a larger value $\nu = 6$ (Fig. 1, left), when the wave function is better approximated near the charge centers, the error due to the approximate treatment of the relativistic singularity [Eq. (16)] becomes smaller also for higher grid point numbers. Here, a suitable distribution of the grid points between the inner and outer regions of the treated domain is achieved [11,17].

In the relativistic shift, one profits from an error cancellation: the error reduces by two or more orders, as the comparison of the green and red lines in Fig. 1 (left) evidences. The scaling of the error of the relativistic shift with grid point number exhibits an exponent of approximately

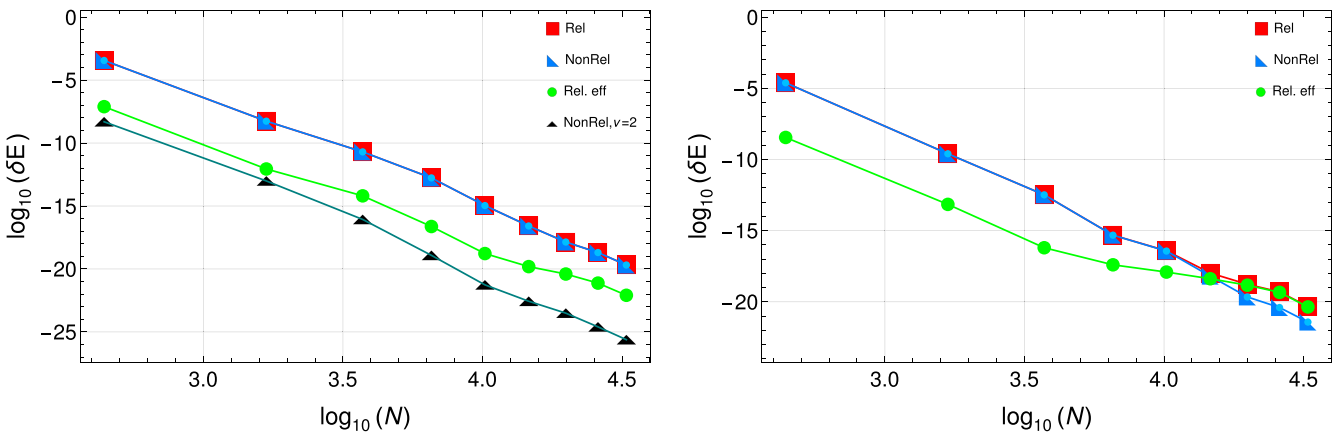

FIG. 1. Convergence behavior of the relativistic (red square) and nonrelativistic (blue, left triangle) energies, and of the relativistic shift (green circle), as a function of the number of grid points, N. $\delta E = E(N) - E$ or $\delta E = \Delta E_{\rm rel}(N) - \Delta E_{\rm rel}$ is the deviation of the energy from the extrapolated value, as given in Table I. Two cases are considered. Left: $D_{\max} = 50$, $\nu = 6$, good convergence. Right: $D_{\max} = 70$, $\nu = 4$, unsatisfactory convergence for the relativistic solution. Left, black triangles: nonrelativistic calculation with $\nu = 2$ and $D_{\max} = 50$.

TABLE II. Dependence of the relativistic shift $\Delta E_{\rm rel}$ (in 10^{-6} atomic units) at $R = 2$ on the domain size $D_{\rm max}$. The second column is the result for the densest grid, with 648/32 761 elements/points. The third column is the extrapolated value for infinite point number. All evaluations were performed with $\nu = 6$. Bold digits are significant.

$D_{\rm max}$	Value for densest grid	Extrapolated value
30	−7.3665376307026089560	**−7.36653763070260**899
40	−7.3665376307026089666	**−7.36653763070260904**
50	−7.3665376307026089298	**−7.36653763070260901**
60	−7.3665376307026088816	**−7.36653763070260**898
70	−7.3665376307026088322	**−7.36653763070260**894

$q \simeq 8.5 < p$. Determining the reason for this is beyond the scope of this work.

We take as the uncertainty of the extrapolated value the difference between the extrapolated value and the value computed for the most dense grid. Then, the achieved uncertainties are as follows. For $E_{\rm rel}$: $\simeq 2 \times 10^{-20}$ atomic units, or $\simeq 2 \times 10^{-20}$ in fractional terms. The same holds for the nonrelativistic energy (with the same ν). For the relativistic shift $\Delta E_{\rm rel} = E_{\rm rel} - E_{\rm nrel}$: $\simeq 1 \times 10^{-22}$ atomic units or $\simeq 1 \times 10^{-17}$ in fractional terms.

To show that the precise value of $D_{\rm max}$ is not crucial, we present in Table II the values of the relativistic shifts for several grid extensions $D_{\rm max}$, and where the grid point number is the largest one reported in Table I. As expected, the shifts stay stable over a large range of $D_{\rm max}$. A larger number of grid points requires larger $D_{\rm max}$ to avoid truncation errors. However, a larger value $\nu = 6, 8, \ldots$ condenses the points in the inner region and dilutes them in the outer region. To counter this effect, one chooses a smaller $D_{\rm max}$ for larger ν for the same system and grids sequence. Note that the variation of $D_{\rm max}$ mainly affects the outer region; therefore, due to the error cancellation, the relativistic shift is less sensitive to $D_{\rm max}$.

Finally, we consider the nonrelativistic calculation. Because the wave function is not singular at the nuclei, $\nu = 2$ is sufficient. This maintains the uniform distribution of the grid points. The wave-function error is determined by the polynomial approximation. As Fig. 1 (black triangles) shows, the convergence order is approximately $q = 9.5$ for large grid point number, almost equal to the polynomial order $p = 10$. Test calculations similar to those in Table II showed that the most accurate result is found for $D_{\rm max} \simeq 50$, yielding the result shown in Table I (last line).

C. Test of the numerical procedure on the hydrogenlike ions

We can test our FEM procedures on the hydrogenlike ions since the exact solution of the Dirac equation is available. The energy levels are given by (in explicit units, excluding the rest-mass energy)

$$E_{jn} = -m_e c^2 \left\{ 1 - \left[1 + \left(\frac{Z\alpha}{(n - j - 1/2) + \sqrt{(j + 1/2)^2 - (Z\alpha)^2}} \right)^2 \right]^{-1/2} \right\}. \tag{17}$$

The relativistic energy shift in atomic units is $\Delta E_{\rm rel} = E_{jn}/(1\,\text{a.u.}) - E_{\rm nrel} = (m_e c^2 \alpha^2)^{-1} E_{jn} + Z^2/(2n^2)$. Here, we consider the ground state, $n = 1$, $j = 1/2$.

The FEM values were computed by setting the second center to be a dummy center with $Z_2 = 0$. In Table III, we show the results for various values of Z_1, each obtained with

TABLE III. Comparison of the extrapolated FEM numerical results for the relativistic shift of hydrogenlike ions with the exact result. Z is the nuclear charge. Exact values are computed using Eq. (17). The cases $Z = 1, 2$ are computed with two different values of c. The first value used is for ease of comparison with other values reported in the literature. The next-to-last entry shows the actual relativistic energies. The last entry reports a nonrelativistic calculation. FEM parameters used: superscript [1]: $D_{\rm max} = 50$, $\nu = 4$; superscript [2]: $D_{\rm max} = 40$, $\nu = 6$; superscript [3]: $D_{\rm max} = 30$, $\nu = 6$.

Z	$\Delta E_{\rm rel}$, exact (a.u.)	$\Delta E_{\rm rel}$, FEM (a.u.)	Difference (a.u.)	note
		$\alpha^{-1} = 137.0359895$		
1	$-6.65659748374605054203 \times 10^{-6}$	$\mathbf{-6.6565974837460505}39 \times 10^{-6}$	-3.0×10^{-24}	[1]
2	$-1.06514068278487728906 \times 10^{-4}$	$\mathbf{-1.0651406827848772}81 \times 10^{-4}$	-1.0×10^{-22}	[1]
		$\alpha^{-1} = 137.035999084$		
1	$-6.656596552625364279 0 \times 10^{-6}$	$\mathbf{-6.6565965526253642}81 \times 10^{-6}$	-2.0×10^{-24}	[2]
2	$-1.06514053378176276 0 \times 10^{-4}$	$\mathbf{-1.0651405337817627}61 \times 10^{-4}$	2.2×10^{-22}	[3]
10	$-6.674201689468916918 \times 10^{-2}$	$\mathbf{-6.6742016894689169}13 \times 10^{-2}$	-4.8×10^{-20}	[3]
20	−1.076523210794734716	**−1.07652321079473471**3	-3.1×10^{-18}	[3]
30	−5.524906318343685119	**−5.52490631834368509**	-3.0×10^{-17}	[3]
	$E_{\rm rel}$, exact	$E_{\rm rel}$, FEM	Difference	
30	−455.52490631834368512	**−455.5249063183436834**	-1.7×10^{-15}	[3]
	$E_{\rm nrel}$, exact	$E_{\rm nrel}$, FEM	Difference	
30	−450	**−449.99999999999998**309	-6.9×10^{-16}	[3]

TABLE IV. FEM nonrelativistic energy of a particular excited state of the two-center problem with $Z_1 = 3, Z_2 = 2$ and distance $R = \sqrt{15}$, that has the exact energy $-(1/2)$ a.u. The third column shows the differences FEM minus exact. The FEM computations were performed with $D_{\max} = 50$, $\nu = 4$. N_e/N is the number of the grid elements/points. The values are truncated.

N_e/N	$E_{\rm nrel}$, FEM (a.u.)	Difference (a.u.)
8/441	−0.493598112780690785516	6.4×10^{-4}
32/1681	−0.499996685189264323528	3.2×10^{-7}
72/3721	−0.499999998831658333453	1.2×10^{-9}
128/6561	0.499999999995025573402	$5. \times 10^{-12}$
200/10201	−0.499999999999921236179	7.9×10^{-14}
288/14641	−0.499999999999998240336	1.8×10^{-15}
392/19881	−0.499999999999999914507	8.5×10^{-17}
512/25921	−0.499999999999999994099	5.9×10^{-18}
648/32761	−0.499999999999999999158	8.4×10^{-19}
extrpl	−0.499999999999999999483	5.1×10^{-20}

10th-order FEM, with the maximum number of grid points computed being 32 761, and extrapolated.

The agreement with the exact results is excellent. For the case of nuclear charge $Z_1 = 1$, the difference of the relativistic shifts is of the order of 10^{-24} a.u., or 5×10^{-19} fractionally. This value confirms our uncertainty estimate given above for the two-center system $H_2{}^+$. The last two entries in the table compare the result of the energies for the relativistic and nonrelativistic cases. We see that our FEM is almost as accurate in the relativistic case as in the nonrelativistic case; there is only a factor 2 loss in accuracy.

Note that unlike what is obviously the case in Eq. (17), in the FEM computations of both the hydrogenic ions and the two-center problem, varying Z_1 or Z_1, Z_2 simultaneously is not equivalent to varying α (such a variation is reported in Table XI below). This is because our computations of the α dependence are based on Eq. (9) with fixed atomic energy unit and atomic distance unit.

D. Test of the numerical procedure on an exactly known excited nonrelativistic molecular state

It is little known that there exist exact solutions of the nonrelativistic two-center problem for particular combinations of charge values Z_1, Z_2 and distances R [24]. These solutions are of great interest because performing the corresponding FEM calculation allows one to verify the extrapolation procedure and the uncertainty estimate. Unfortunately, these exact solutions are not the electronic ground states, but excited states. We have treated the case ($Z_1 = 3$, $Z_2 = 2$, $R = \sqrt{15}$), whose $4s\sigma$ state has the exact nonrelativistic electronic energy, $E_{\rm nrel} = -(1/2)$ a.u. The FEM computation is very cumbersome because this state is the 21st $j_z = 1/2$ state in order of increasing energy, and all intermediate states have to be calculated before treating the state of interest. As for other calculations in the present study, the energy values are iterated until they remain stable at the level of $\sim 10^{-27}$–10^{-30} a.u.

The result is shown in Table IV. The difference of the extrapolated value relative to the exact value is 5×10^{-20} a.u. This agreement, obtained for a system having substantially larger squared charge than the $H_2{}^+$ system, comparatively large ground-state energy -5.01691106677841796618 a.u. (significant digits, extrapolated), and using a moderate value of $D_{\max}$, gives us confidence that our uncertainty estimates for the relativistic solution of $H_2{}^+$ are reasonable.

IV. RESULTS

A. Series expansion of the relativistic shift

We have computed the FEM relativistic energy shift at $R = 2$ a.u. for a set of values of $c = \alpha^{-1}$, ranging from 5 to 1200. The shifts are reported in Table XI. We fitted a series $\Delta E_{\rm rel} = \sum_{s=1}^{s_{\max}} d_{2s}\alpha^{2s}$ to the FEM data. The best-fitting series is with $s_{\max} = 6$ and is reported in Table V, together with the standard errors of the best-fit coefficients. The resulting fractional deviations of the fitted values from the FEM values are approximately $(1$–$10)\times 10^{-16}$, substantially larger than the uncertainties of the FEM values. Therefore, these FEM uncertainties were not taken into account in the fit.

We also show in Table V the comparison of our best-fit series expansion with what we believe is the most precise perturbation series. The coefficient for the order α^2 was recently recomputed by Korobov [27]. It differs by 7×10^{-12} a.u. from the value in the supplemental material of Korobov (2018) (file "tmph-2017-0313-File001.dat") [25]. It is now in agreement with the FEM-computed coefficient. We recognize that a main difference between the perturbation result and FEM result is the coefficient of the order of α^4. The uncertainty of the perturbation coefficient value as calculated

TABLE V. Numerical series expansion of the FEM relativistic shift $\Delta E_{\rm rel}$ and comparison with perturbation and variational theory results. Column 2 contains the coefficients d_{2s}, $s = 1, \ldots, 6$, for $H_2{}^+$ at $R = 2$ a.u. Columns 3 and 4 list the available best results of perturbation and variational theory, respectively. Column 5 shows rounded values of the coefficients for the exact solution of the hydrogen atom. The uncertainties in column 2 are for the 95% confidence intervals. The uncertainty in column 3, line 3 is one unit of the last digit. [a] Ref. [27]; [b] Ref. [10]; [c] Ref. [26].

Term	Coefficient (a.u.)			
	This work	Perturbation theory	Variational	Hydrogen atom
α^2	−0.1383329938679795656 ± 2.6×10⁻¹⁸	−0.138332993868 [a]		−0.125
α^4	−0.04172790053721 (3 ± 5)	−0.041711 [b]		−0.0625
α^6	−0.02831842636 (64 ± 31)		−0.0286(5) [c]	−0.0390625
α^8	−0.020829172 (3 ± 7)			−0.0273438
α^{10}	−0.0159689 (1 ± 5)			−0.0205078
α^{12}	−0.013452 (8 ± 9)			−0.0161133

TABLE VI. Relativistic shift $\Delta E_{\rm rel}$, in units 10^{-6} a.u., as a function of internuclear distance. $\alpha^{-1} = 137.035999084$. The calculation is performed with $D_{\rm max} = 35$, $\nu = 8$ in the range $R = 0.05$–0.25, $D_{\rm max} = 40$, $\nu = 8$ in the range $R = 0.30$–1.95, and with $D_{\rm max} = 40$, $\nu = 6$ for $R = 2.0$–5.0, and in addition extrapolated to infinite grid point density.

R	$\Delta E_{\rm rel}(R)$	R	$\Delta E_{\rm rel}(R)$	R	$\Delta E_{\rm rel}(R)$	R	$\Delta E_{\rm rel}(R)$
0.05	−102.205220874297353	1.30	−12.448456768274240	2.55	−5.97244880905323561	3.80	−5.28072339944993510
0.10	−94.2070961513458068	1.35	−11.840587433312817	2.60	−5.89682181016418189	3.85	−5.28498620517162691
0.15	−85.3131813342957982	1.40	−11.287362392410170	2.65	−5.82730252634455702	3.90	−5.29060881471213234
0.20	−76.6282196861760657	1.45	−10.783014143550542	2.70	−5.76349219079285695	3.95	−5.29751088104089074
0.25	−68.6084308516448949	1.50	−10.322491660645794	2.75	−5.70502398629843855	4.00	−5.30561552816506309
0.30	−61.4076071297781014	1.55	−9.9013599726656259	2.80	−5.65155994593625421	4.05	−5.31484911635246100
0.35	−55.0368465872734128	1.60	−9.5157152038954672	2.85	−5.60278818603095446	4.10	−5.32514103071051427
0.40	−49.4432261483497075	1.65	−9.1621125180967957	2.90	−5.55842043205063507	4.15	−5.33642349106801577
0.45	−44.5490384746501491	1.70	−8.8375048531073833	2.95	−5.51818980322643993	4.20	−5.34863138128002584
0.50	−40.2710819788872559	1.75	−8.5391906977447463	3.00	−5.48184882610666476	4.25	−5.36170209623029187
0.55	−36.5297231045446188	1.80	−8.2647694632039667	3.05	−5.44916765105193533	4.30	−5.37557540494242218
0.60	−33.2527185045808470	1.85	−8.0121032479359465	3.10	−5.41993244895295341	4.35	−5.39019332833313161
0.65	−30.3763935052245251	1.90	−7.7792839978640807	3.15	−5.39394396828117659	4.40	−5.40550003025016080
0.70	−27.8455359036944480	1.95	−7.5646052307100206	3.20	−5.37101623503049416	4.45	−5.42144172053575057
0.75	−25.6127144763335920	2.00	−7.3665376307026090	3.25	−5.35097538022926582	4.50	−5.43796656894539199
0.80	−23.6373874480319195	2.05	−7.1837079333992589	3.30	−5.33365858154336776	4.55	−5.45502462883235896
0.85	−21.8849832650076221	2.10	−7.0148806141308055	3.35	−5.31891310709145427	4.60	−5.47256776958247562
0.90	−20.3260390746755839	2.15	−6.8589419712531499	3.40	−5.30659545098689629	4.65	−5.49054961685173189
0.95	−18.9354315392755268	2.20	−6.7148862598532203	3.45	−5.29657055133523823	4.70	−5.50892549972265814
1.00	−17.6917086864986668	2.25	−6.5818035851749282	3.50	−5.28871108247578041	4.75	−5.52765240395459001
1.05	−16.5765189239048591	2.30	−6.4588693097269201	3.55	−5.28289681418178407	4.80	−5.54668893055877092
1.10	−15.5741278636581426	2.35	−6.3453347653767748	3.60	−5.27901403134357336	4.85	−5.56599525898221531
1.15	−14.6710118162609399	2.40	−6.2405190930066166	3.65	−5.27695500836772192	4.90	−5.58553311423485584
1.20	−13.8555168671494631	2.45	−6.1438020585500913	3.70	−5.27661753314668177	4.95	−5.60526573734309895
1.25	−13.1175733519842682	2.50	−6.0546177163079877	3.75	−5.27790447599794821	5.00	−5.62515785855980919

by Korobov is not known. However, our result for the α^6-order coefficient confirms the value and uncertainty estimate of Mark and Becker [26]. In total, at $R = 2$ a.u., the FEM result is approximately 0.3 kHz smaller than the perturbation result.

B. Electronic binding energy curve

The R dependence of the Dirac energy for H_2^+ has received little attention after the early works by Luke *et al.* [28] and Bishop [29] because, after the experiment of Wing *et al.* in 1976 [30], for several decades no precision spectroscopy experiments were performed that could challenge the theory. The work of Howells and Kennedy is one of the few exceptions [31]. In the early 2000s, Korobov computed the R-dependent precise perturbation theory in connection with the new generation of experiments that had started. The result consists of the α^2 coefficient [9], whose updated values have been provided by Korobov for this work, and the α^4 coefficient [10,25]. We denote the relativistic shift computed from this data by $\Delta E_{\rm rel,Korobov}$.

We have computed by FEM the relativistic shift for R values from $R = 0.05$ to $R = 5.0$ in steps of 0.05; see Table VI. From the smallest to the largest R, the absolute uncertainties vary from 7×10^{-20} to 1.2×10^{-23}, i.e., from 7×10^{-16} to 3×10^{-18} in fractional terms.

TABLE VII. Comparison of present and literature values for the ground-state energy of the H_2^+ molecular ion at $R = 2$. This work: FEM result computed with $\nu = 6$, $D_{\rm max} = 40$. All results were obtained for $\alpha^{-1} = 137.0359895$.

Reference	$E_{\rm rel}$
This work	−1.10264158103360758005
Mironova *et al.* (2015) [37]	−1.1026415810330
Tupitsyn *et al.* (2014) [38]	−1.1026415810330
Fillion-Gourdeau *et al.* (2012) [39]	−1.102641580782
Artemyev *et al.* (2010) [40]	−1.1026409
Ishikawa *et al.* (2008) [41]	−1.102641581033598
Kullie and Kolb (2001) [11]	−1.10264158103358
Parpia and Mohanty (1995) [42]	−1.1026415801
Sundholm (1994) [43]	−1.102641581
Yang *et al.* (1991) [34]	−1.1026415810336

V. DISCUSSION AND CONCLUSION

A. Comparison with other work

Historically, the first numerical solution of the Dirac equation for the two-center problem was undertaken by Pavlik and Blinder [32], followed by Luke *et al.* [28] and by Müller *et al.* [33]. Two decades later, the precision had improved by five orders with the work of Yang *et al.* [34]. Another one order of improvement followed in the next decade, reported by Kullie and Kolb [11]. In the two decades from that work until the present work, no other independent result was published with comparable or lower uncertainty, to the best of our knowledge. Several studies of the Dirac equation were undertaken, but

TABLE VIII. Some results on the relativistic shift at $R = 2$ a.u. The value of α used for the computation is indicated. "Rescaled" means that the original computation was made for a different value of α. We rescaled the original value of the shift by $(\alpha/\alpha_{\rm orig})^2$ in order to allow comparison of the shift values. This rescaling is adequate, given the moderate number of significant digits in the quoted works. The uncertainty indicated in parentheses is either taken from a statement of the authors or, in absence, the unit of the last digit of the reported shift value is assumed. Notation: "7.38(3)" means an uncertainty of 0.03.

Authors	$-10^6\ \Delta E_{\rm rel}$ (a.u.)	α^{-1}	Comment
Pavlik and Blinder 1967	7.2(1)	137.036	
Luke et al. 1969	7.38(3)	137.03600	rescaled
Bishop 1977	7.381(5)	137.036	
Mark and Becker 1987	7.366(1)	137.0359991	rescaled
Sundholm 1987	7.3656(1)	137.0359990840	rescaled
Rutkowski and Rutkowska 1987	7.3635(1)	137.0359990840	rescaled
Yang et al. 1991	7.3665377(1)	137.0359990840	rescaled
Kullie and Kolb, 2001	7.36653760(1)	137.0359990840	rescaled
Korobov and Tsogbayar 2007 Mark and Becker 1987 Korobov 2022	7.366537583(3)	137.0359990840	pert. theory, variational calc.
Mironova et al 2015	7.3665371(1)	137.0359990840	rescaled
this work	7.36653763070260900(7)	137.0359990840	

they were not aimed towards record precision for the H_2^+ system. Table VII presents some results on the total energy that were published in the last 25 years. For earlier listings of results on the Dirac equation for H_2^+, see, e.g., Rutkowski and Rutkowska [35], Sundholm [36], and Mironova *et al.* [37]. Table VIII instead focuses on the relativistic shift, going back to the earliest works. We see that the present result is not or only marginally in agreement with Refs. [10,11,37], perhaps because their uncertainties were underestimated.

Figure 2 plots in red the difference between the FEM result and $E_{\rm rel,Korobov}$ for some of the available values of R. The same value of c is used. The difference is less than 1.5 kHz in magnitude for the range of R values where the considered nuclear wave functions have significant probability. Note that the uncertainty of the FEM values is estimated to be of the order of 10^{-22} a.u. $\simeq 10^{-9}$ kHz, completely negligible on the scale of the plot. We have not analyzed the origin of the visible small deviations of the values from a smooth dependence, especially near $R = 1$, as they do not impact the following discussion. For concreteness, Table IX compares our values of the relativistic shift with the previous result, for selected values of internuclear distance.

TABLE IX. Relativistic shifts: column 2 is the perturbation results $\Delta E_{\rm rel,Korobov}$; column 3 is the deviations of the FEM results, $\Delta E_{\rm rel}$, from the perturbation results. For the FEM values, see Table VI. Note: 1×10^{-14} a.u. corresponds to 66 Hz.

R	$\Delta E_{\rm rel,Korobov}$ (10^{-6} a.u.)	$\Delta E_{\rm rel} - \Delta E_{\rm rel,Korobov}$ (10^{-14} a.u.)
0.5	−40.2710800643	−193.577
1.0	−17.6917083247	−36.1806
2.0	−7.36653763008	−4.9999
3.0	−5.48184882611	−1.77565
4.0	−5.30561552817	−1.21509
5.0	−5.62515785856	−0.522041

B. Relativistic shift of transition frequencies

A key question is whether the highly accurate results obtained in this work affect the interpretation of the experiments performed so far. Those interpretations were based on the theoretical treatment of Korobov [1] and co-workers.

We compute the relativistic shift to any rotational-vibrational level energy as the average over the nuclear rotational-vibrational probability density,

$$\Delta E_{\rm rel}(v, L) = \int_{R_{\rm min}}^{R_{\rm max}} \Delta E_{\rm rel}(R)[\psi_{v,L}(R)]^2 R^2 dR. \qquad (18)$$

Here, $\psi_{v,L}(R)$ is the nuclear wave function, and v, L are the vibrational and rotational quantum numbers of the level. The

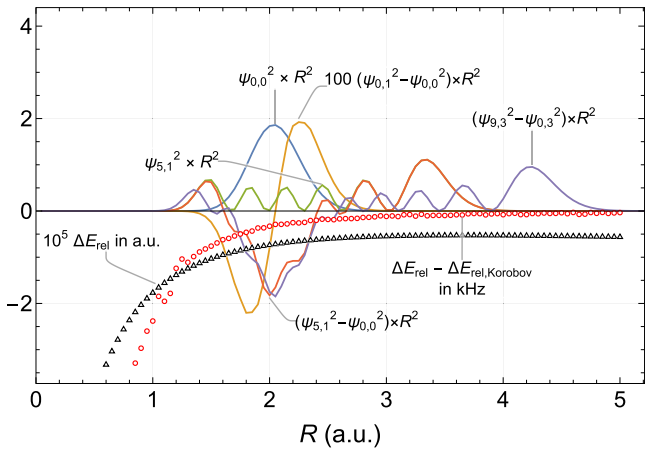

FIG. 2. Black triangles: FEM relativistic energy shift $\Delta E_{\rm rel}$ for the two-center problem as a function of nuclear distance R. Red circles: difference between FEM and perturbation theory. The units of these two quantities are stated in the labels. The values of a selection of red circle points is given in column 3 of Table IX. Other lines: the nuclear radial probability densities and density differences for some relevant rotational-vibrational levels and transitions of the HD^+ molecule.

TABLE X. Correction $\delta\nu$ to the transition frequencies of HD^+ arising from the present treatment of the relativistic shift, *to be added* to the perturbation result of Korobov. The fractional correction is the contribution normalized to the respective transition frequency.

Transition	Correction $\delta\nu$ (Hz)	Fractional correction
$(v=0, L=0) \to (v'=0, L'=1)$	0.9	7×10^{-13}
$(v=0, L=0) \to (v'=5, L'=1)$	60	2×10^{-13}
$(v=0, L=3) \to (v'=9, L'=3)$	110	3×10^{-13}

relativistic shift of a transition frequency between an upper level (v', L') and a lower level (v, L) is $\Delta\nu_{\rm rel}(v, L, v', L') = \Delta E_{\rm rel}(v', L') - \Delta E_{\rm rel}(v, L)$. This relativistic shift is not complete: there are finite-nuclear-mass corrections to it. However, the fixed-nuclei shifts that we treat here are the dominant ones. As they turn out to be small (see below), we do not need to consider their corrections.

We apply this expression to the molecule HD^+, since precision spectroscopic results on rovibrational transitions are so far available only for it. The range $\{R_{\rm min}, R_{\rm max}\}$ over which we computed the relativistic energy shift is sufficiently large for the levels investigated experimentally so far. The HD^+ wave functions $\psi_{v,L}(R)$ were obtained by averaging over the electronic degrees of freedom the full nonrelativistic three-body wave function computed by Korobov.

We show in Fig. 2 the differences between the squared wave functions of a few levels that have recently been studied experimentally. Because these differences oscillate as a function of R and because the theory difference $\Delta E_{\rm rel} - \Delta E_{\rm rel,Korobov}$ is a slowly varying function over the range of R values where the levels in question have a substantial probability density, the differences (corrections) $\delta\nu = \Delta\nu_{\rm rel} - \nu_{\rm rel,Korobov}$ turn out to be small. The values are reported in Table X.

We conclude that the corrections $\delta\nu$ are negligible compared to today's uncertainty of the QED contributions, which amount to $\simeq 1 \times 10^{-11}$ relative to the transition frequencies. Nevertheless, we expect that in the not-too-distant future, the precise results obtained here will become relevant, given that the QED calculations may improve and that experiments definitely have the potential to improve their precision by several

TABLE XI. Energy and relativistic shift at $R = 2$ a.u. for different values of $c = \alpha^{-1}$. Values $E_{\rm rel}$, $\Delta E_{\rm rel}$ are extrapolations to an infinitely dense grid. Column 4 lists the estimated uncertainty of the relativistic shift, $u(\Delta E_{\rm rel})$, where the notation (X) stands for $\times 10^X$. C18 = 137.035999084 is the CODATA 2018 value. For $\alpha^{-1} = 5$–100, the calculations were performed with $D_{\rm max} = 40$, $\nu = 8$; for the remaining values, $D = 50$, $\nu = 6$ was used. The uncertainty is estimated as $u = |\Delta E_{\rm rel} - \Delta E_{\rm rel}\,(\text{densest grid})|$.

c	$E_{\rm rel}$ (a.u.)	$\Delta E_{\rm rel}$ (10^{-6} a.u.)	u (a.u.)	c	$E_{\rm rel}$ (a.u.)	$\Delta E_{\rm rel}$ (10^{-6} a.u.)	u (a.u.)
5	−1.10823616628281245725	−5601.95178786599669	1(-20)	160	−1.10263961819119284065	−5.40369624637914234	5(-23)
10	−1.10402174575200841030	−1387.53125706194975	2(-21)	170	−1.10263900115369296245	−4.78665874650093787	4(-23)
15	−1.10324985455012380333	−615.640055177342779	9(-22)	180	−1.10263848407154501463	−4.26957659855311778	3(-23)
20	−1.10298030822228538131	−346.093727338920758	5(-22)	190	−1.10263804646585469507	−3.83197090823356170	3(-23)
25	−1.10285565422468955126	−221.439729743090708	3(-22)	200	−1.10263767284587354132	−3.45835092707980879	3(-23)
30	−1.10278796937627037902	−153.754881323918467	2(-22)	250	−1.10263642783353080771	−2.21333858434620445	1(-23)
35	−1.10274716721032824078	−112.952715381780223	1(-22)	300	−1.10263575153336329279	−1.53703841683127793	1(-23)
40	−1.10272068892299195324	−86.4744280454926898	1(-22)	350	−1.10263534374665671285	−1.129251710251342481	8(-24)
45	−1.10270253726390794456	−68.3227689614840043	8(-23)	400	−1.10263507907778813941	−0.864582841677900829	6(-24)
50	−1.10268955437077065101	−55.3398758241904579	7(-23)	450	−1.10263489762185970781	−0.683126913246303846	4(-24)
55	−1.10267994897141281291	−45.7344764663523530	5(-23)	500	−1.10263476782758958165	−0.553332643120139307	3(-24)
60	−1.10267264354692895289	−38.4290519824923411	4(-23)	550	−1.10263467179455575659	−0.457299609295080670	2(-24)
65	−1.10266695836994784029	−32.7438750013797330	3(-23)	600	−1.10263459875358473660	−0.384258638275091429	2(-24)
70	−1.10266244745636394391	−28.2329614174833596	3(-23)	650	−1.10263454191055032518	−0.327415603863668284	1(-24)
75	−1.10265880834615650990	−24.5938512100493472	2(-23)	700	−1.10263449680735263922	−0.282312406177710643	1(-24)
80	−1.10265583004409394271	−21.6155491474821583	2(-23)	750	−1.10263446042040077440	−0.245925454312894882	1(-24)
85	−1.10265336172953448692	−19.1472345880263714	2(-23)	800	−1.10263443064035125509	−0.216145404793583294	1(-24)
90	−1.10265129327838995379	−17.0787834434932376	1(-23)	850	−1.10263440595937777350	−0.191464431311990959	8(-25)
95	−1.10264954276284737702	−15.3282679009164686	1(-23)	900	−1.10263438527648397256	−0.170781537511048560	7(-25)
100	−1.10264804821164058439	−13.8337166941238396	1(-23)	950	−1.10263436777255322485	−0.153277606763340967	5(-25)
110	−1.10264564725880168723	−11.4327638552257233	1(-22)	1000	−1.10263435282798205741	−0.138333035595908438	5(-25)
120	−1.10264382115409753260	−9.60665915107108865	9(-23)	1050	−1.10263433996708407279	−0.125472137611282305	4(-25)
130	−1.10264240002530585058	−8.18553035938906732	7(-23)	1100	−1.10263432881976328289	−0.114324816821377799	3(-25)
C18	−1.10264158103257716412	−7.36653763070260900	7(-23)	1150	−1.10263431909458761106	−0.104599641149552752	3(-25)
140	−1.10264127240938096226	−7.05791443450075182	6(-23)	1200	−1.10263431055954565992	−0.096064599198404129	2(-25)
150	−1.10264036271043522934	−6.14821548876783325	5(-23)				

orders. Another application of the present results is to use the obtained wave functions to compute quantities of relevance for a more precise treatment of the QED corrections.

Note added: Extending Table I, we obtained the energies for an even larger grid, $N_e/N = 800/40401$, using $D = 50$, $\nu = 6$, $\alpha = 137.035999084$. The more precise extrapolated values are $E_{\rm rel} = -1.10264158103257716411725691$, $E_{\rm nrel} = -1.10263421449494646150814441 0$, $\Delta E_{\rm rel} = -7.36653763070260911 \times 10^{-6}$. The value $\Delta E_{\rm rel}$ has an estimated uncertainty of 2.3×10^{-23} a.u., fractionally 3×10^{-18}.

ACKNOWLEDGMENTS

We are very grateful to V. I. Korobov for motivating the subject of this work, providing precise nonrelativistic results, updated values of his earlier relativistic calculations, and the vibrational wave functions. One of us (O.K.) thanks Professor D. Kolb for discussions and Professor M. Garcia at the Universität Kassel for his support. We also thank the computing centers at Universität Kassel and Universität Düsseldorf for providing resources and advice. This work was supported the European Research Council (ERC) under the European Union's Horizon 2020 research and innovation program (Grant No. 786306, "PREMOL").

[1] V. I. Korobov and J.-P. Karr, Phys. Rev. A **104**, 032806 (2021).
[2] S. Alighanbari, G. S. Giri, F. L. Constantin, V. I. Korobov, and S. Schiller, Nature (London) **581**, 152 (2020).
[3] I. V. Kortunov, S. Alighanbari, M. G. Hansen, G. S. Giri, V. I. Korobov, and S. Schiller, Nat. Phys. **17**, 569 (2021).
[4] S. Patra, M. Germann, J.-P. Karr, M. Haidar, L. Hilico, V. I. Korobov, F. M. J. Cozijn, K. S. E. Eikema, W. Ubachs, and J. C. J. Koelemeij, Science **369**, 1238 (2020).
[5] S. Alighanbari, I. V. Kortunov, G. Giri, V. I. Korobov, and S. Schiller (unpublished).
[6] A. D. Ludlow, M. M. Boyd, J. Ye, E. Peik, and P. O. Schmidt, Rev. Mod. Phys. **87**, 637 (2015).
[7] C. Wellers, M. R. Schenkel, G. S. Giri, K. R. Brown, and S. Schiller, Mol. Phys. e2001599 (2021).
[8] S. Schiller, D. Bakalov, and V. I. Korobov, Phys. Rev. Lett. **113**, 023004 (2014).
[9] T. Tsogbayar and V. I. Korobov, J. Chem. Phys. **125**, 024308 (2006).
[10] V. I. Korobov and T. Tsogbayar, J. Phys. B: At. Mol. Opt. Phys. **40**, 2661 (2007).
[11] O. Kullie and D. Kolb, Eur. Phys. J. D **17**, 167 (2001).
[12] O. Kullie and D. Kolb, J. Phys. B: At. Mol. Opt. Phys. **36**, 4361 (2003).
[13] O. Kullie, D. Kolb, and A. Rutkowski, Chem. Phys. Lett. **383**, 215 (2004).
[14] J. Dolbeault, M. J. Esteban, E. Séré, and M. Vanbreugel, Phys. Rev. Lett. **85**, 4020 (2000).
[15] J. D. Talman., Phys. Rev. Lett. **57**, 1091 (1986).
[16] J. Dolbeault, M. Esteban, and E. Séré, J. Funct. Anal. **174**, 208 (2000).
[17] O. Kullie, Ph.D. thesis, Universität Kassel, 2004, http://nbn-resolving.de/urn:nbn:de:hebis:34-1835.
[18] D. Heinemann, Ph.D. thesis, Universität Kassel, 1987.
[19] H. Zhang, O. Kullie, and D. Kolb, J. Phys. B: At. Mol. Opt. Phys. **37**, 905 (2004).
[20] L. Yang, D. Heinemann, and D. Kolb, Phys. Rev. A **48**, 2700 (1993).
[21] C. Düsterhöft, D. H. L. Yang, and D. Kolb, Chem. Phys. Lett. **229**, 667 (1994).
[22] A two-variable, p-order, complete polynomial is, by definition, $a_{00} + a_{10}\, s + a_{01}\, t + a_{11}\, s\, t + a_{20}\, s^2 + a_{02}\, t^2 + \cdots + a_{p0}\, s^p + a_{0p}\, t^p$.
[23] L.-J. Yang, Ph.D. thesis, Universität Kassel, 1991.
[24] Yu. N. Demkov, JETP Lett. **7**, 76 (1968).
[25] V. I. Korobov, Mol. Phys. **116**, 93 (2018).
[26] F. Mark and U. Becker, Phys. Scr. **36**, 393 (1987).
[27] V. I. Korobov (private communication).
[28] S. K. Luke, G. Hunter, R. P. McEachran, and M. Cohen, J. Chem. Phys. **50**, 1644 (1969).
[29] D. M. Bishop, J. Chem. Phys. **66**, 3842 (1977).
[30] W. H. Wing, G. A. Ruff, W. E. Lamb, and J. J. Spezeski, Phys. Rev. Lett. **36**, 1488 (1976).
[31] M. H. Howells and R. A. Kennedy, J. Chem. Soc., Faraday Trans. **86**, 3495 (1990).
[32] P. I. Pavlik and S. M. Blinder, J. Chem. Phys. **46**, 2749 (1967).
[33] B. Müller, J. Rafelski, and W. Greiner, Phys. Lett. B **47**, 5 (1973).
[34] L. Yang, D. Heinemann, and D. Kolb, Chem. Phys. Lett. **178**, 213 (1991).
[35] A. Rutkowski and D. Rutkowska, Phys. Scr. **36**, 397 (1987).
[36] D. Sundholm, P. Pyykko, and L. Laaksonen, Phys. Scr. **36**, 400 (1987).
[37] D. Mironova, I. Tupitsyn, V. Shabaev, and G. Plunien, Chem. Phys. **449**, 10 (2015).
[38] I. Tupitsyn and D. Mironova, Opt. Spectrosc. **117**, 351 (2014).
[39] F. Fillion-Gourdeau, E. Lorin, and A. D. Bandrauk, Phys. Rev. A **85**, 022506 (2012).
[40] A. N. Artemyev, A. Surzhykov, P. Indelicato, G. Plunien, and T. Stöhlker, J. Phys. B: At. Mol. Opt. Phys. **43**, 235207 (2010).
[41] A. Ishikawa, H. Nakashima, and H. Nakatsuji, J. Chem. Phys. **128**, 124103 (2008).
[42] F. A. Parpia and A. Mohanty, Chem. Phys. Lett. **238**, 209 (1995).
[43] D. Sundholm, Chem. Phys. Lett. **223**, 469 (1994).